# An In Vitro Fluid Dynamic Study of Pediatric Cannulae: The Value of Animal Studies to Predict Human Flow

**Tobias C. Long**

**Joseph J. Pearson**

**Andrew C. Hankinson**

**Steven Deutsch**

**Keefe B. Manning**[1]

Department of Bioengineering,
The Pennsylvania State University,
University Park, PA 16802

*A challenge to the development of pediatric ventricular assist devices (PVADs) is the use of the aortic cannulae attached to the devices. Cannulae used for pediatric application have small diameters and large pressure drops. Furthermore, during the development of the 12cc Penn State pediatric PVAD, particle image velocimetry (PIV) illustrated that hematocrit levels, through changes in blood viscoelasticity, affected the fluid dynamics. The objective of this study is to compare the fluid dynamics of a pediatric viscoelastic blood analog and a goat viscoelastic blood analog within the PVAD aortic cannula. Two acrylic models were manufactured to model the aortic cannula (6 mm and 8 mm diameters). PIV data was collected to examine the flow at the outlet of the VAD and in the aortic cannula at heart rates of 50 and 75 beats per minute (bpm). Three planes of data were taken, one at the centerline and two 1.5 mm above and below the centerline. Three more planes of data were taken orthogonal to the original planes. While a 75 bpm heart rate was used to represent normal operating conditions, a 50 bpm heart rate represented use of the PVAD during weaning. At 75 bpm, differences were evident between the two different fluids and the two models. Separation zones developed in the plane below the centerline for the higher hematocrit pediatric blood analog. This study raises question to the usefulness of animal testing results in regard to how well they predict the outcome of pediatric patients.*
[DOI: 10.1115/1.4006428]

*Keywords: pediatric, cannula, pulsatile, hematocrit, mechanical circulatory support, particle image velocimetry, fluid dynamics*

## 1 Introduction

Because of the high mortality rate for pediatric patients on the heart transplant list, ventricular assist devices (VADs) suitable for pediatrics are being developed [1]. VADs are used in adult patients as a viable option for bridge to transplant. Adult VADs have also shown potential for aiding in myocardial recovery [2–4]. Thromboembolism remains the major impediment to successful VAD use and, because of the much smaller size and blood volume of pediatric VADs, the problem will likely be worse in pediatric pumps. Implantation of the Berlin Heart in pediatric patients strongly suggests that this is the case [5–7].

Animal testing of adult VADs has been largely in calves, while the requirement of small blood volume and a relatively slow growth rate has led to the use of lambs or baby goats for pediatric VAD tests [8]. While bovine blood has, from a rheological point of view, properties not unlike human blood, sheep and goat blood behave nearly as Newtonian fluids [9]. For pediatric patients, whose blood hematocrit may vary from 20% to 60% [10], sheep or goat blood is a poor rheological approximation—particularly at the low strain rates of interest in thrombosis, as we illustrate in Fig. 1. This may make the interpretation of animal data more difficult.

Although some work, to highlight the flow field differences inside the VAD as a function of the fluid, has been done through in vitro experiments in our laboratory, the flow in the pediatric VAD is quite complex and its interpretation difficult. Here, we turn to the simpler, though still technologically important, problem of flow through the outlet cannula of the Penn State pulsatile PVAD. The outflow is of particular importance as any mismatch in the seating of the outflow valve and its connection to the cannula may become a site for thrombosis. The subsequent probability of embolization in the flow field dominated by the geometry and motion of the outlet valve is not at all understood.

The geometry of cannulae used for pediatric application has a significant impact on the pressure drop that results from fluid flow [11]. Therefore, some cannula geometries may produce better results than others and this should be considered during the development of the devices. Cannulae geometries have long been examined for non-VAD use [12–14]. For example, catheter geometries were extensively studied after it was found that high local shear stresses and low flow zones in catheters strongly affected blood clot formation. Mareels et al. showed that minor geometrical changes could produce large variations in the fluid dynamics. For example, cutting the catheter end at an angle increased shear stress levels when compared to the straight cut catheter. The blood residence times also varied between the different geometries. The straight cut catheter was the preferred design because it appeared to have the least potential for platelet activation, due to lower shear stresses and local residence times [12]. Muehrcke et al. showed cannula mediated atheroembolism in the ascending aorta. An arterial cannula was designed and compared to several other cannulae already used in the clinic. This cannula, designed to lower the exit force and blood velocity, showed better results during in vitro studies. It was presumed that minimizing exit force and flow velocity would

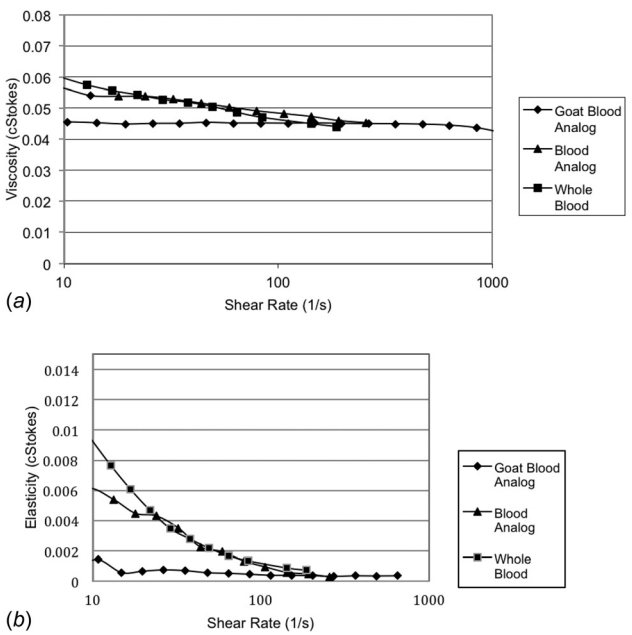


**Fig. 1 Viscosity comparison between the pediatric blood analog, whole pediatric blood, and goat blood**

[1]Corresponding author.

Contributed by the Bioengineering Division of ASME for publication in the JOURNAL OF BIOMECHANICAL ENGINEERING. Manuscript received December 1, 2011; final manuscript received March 15, 2012; accepted manuscript posted March 23, 2012; published online April 18, 2012. Assoc. Editor: Tim David.

  

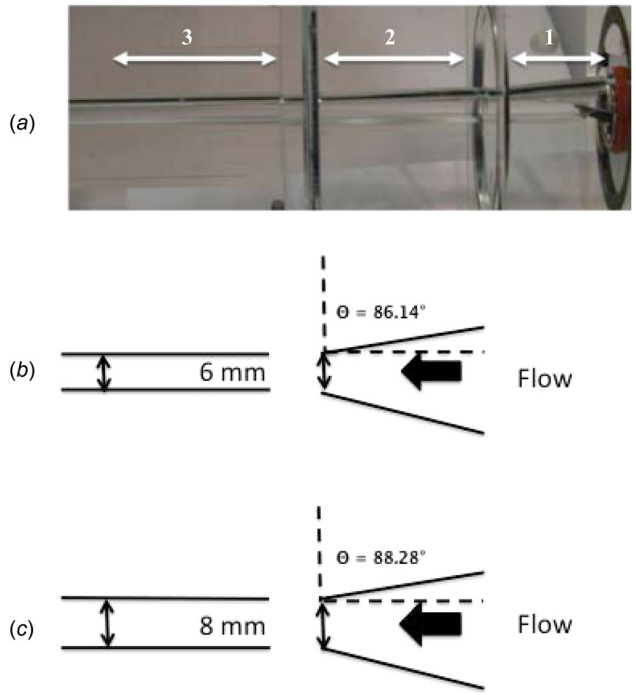


**Fig. 2 Photograph of the acrylic cannula model (*a*). Section 1 (25.4 mm) represents the outlet port of the PVAD which has been made clear for this study. Section 2 (31.75 mm) represents the decreasing diameter within the cannula before it enters the aorta. Section 3 (101.6 mm, not fully shown) represents a continuation of the cannula into the aorta. Fluid flows from right to left in the model. The bottom line-diagram (*b*) and (*c*) demonstrates the difference in the two models.**

decrease the possibility of atheroemboli and stroke [13]. The length and diameter of cannulae can significantly affect pressure drops. It is important to have a low pressure drop to decrease the possibility of blood damage and platelet activation [14].

There have been several studies of pediatric cannulae used in clinical settings. Pediatric cardiopulmonary bypass procedures use aortic and venous cannulae [15]. The size (diameter) and geometries of these cannulae can alter their performance. Pediatric cannulae, being smaller than the adult cannulae, create larger pressure drops and have a greater effect on blood flowing through them [16]. The Berlin Heart Excor cannulae for pediatric patients have diameters of 4.8, 6, and 8 mm; while the adult cannulae have diameters of 12 mm. When compared to the cannulae used in the heart-lung machine, these pediatric cannulae produce little afterload to the native heart. However, the design of the pediatric cannula used in VADs is important for optimizing arterial return. Yang et al. demonstrated that cannula positioning can have an effect on the local fluid dynamics as blood exits the VAD and empties into the aorta [9,17]. Examining and comparing the effects of cannula size on the fluid dynamics of blood flow through them is a second focus of the current work.

Comparisons among cannulae are often made in terms of pressure drop. Detailed measurements of the flow inside a cannula have not been presented. Here, we use particle image velocimetry (PIV) to make detailed flow measurements in several PVAD outlet cannulae for both animal and human blood analogs in an attempt to better understand the difference in flow characteristics.

## 2 Methods

The cannula model (Fig. 2) was made from acrylic to allow for particle image velocimetry (PIV). The model mimicked the geometry from the PVAD outlet to the aortic arch. The model is divided into multiple sections in order to accurately mimic the changing dimensions and separate parts of the PVAD outlet. Section 1 of the model (PVAD outlet port) tapers from the mechanical heart valve outlet 17 mm in diameter to a diameter of 9.5 mm over 25.4 mm, whereby the pediatric cannula would be attached at Sec. 2 in Fig. 2. Section 2 represents the cannula attachment. Two equal length but different diameter sections were made for comparison. The first tapers to a diameter of 6 mm (taper angle 86.14 and the other tapers to a diameter of 8 mm (taper angle 88.28), both over 25.4 mm. The third section continues to follow the cannula dimensions with a 6 mm or 8 mm diameter, respectively, over 101.6 mm. The aortic valve used in the model was the 17 mm Bjork-Shiley Monostrut (BSM) valve with an effective orifice area (EOA) of 1.1 $cm^2$.

The model was placed in a mock circulatory loop similar to the one described by Rosenberg et al., but modified for pediatric application by decreasing the overall volume and increasing the overall resistance [18]. A Harvard Pulsatile Pump was used to run the loop and allow for changes in systolic duration and heart rate. The loop was run at 50 and 75 bpm. Flow rates and outlet pressures were matched to physiological conditions. At 75 bpm, data were collected with a flow rate of 1.4 L/min, outlet pressures of 90/60 mmHg, and a systolic duration of 340 ms. At 50 bpm, data were collected with a flow rate of 0.85 L/min, outlet pressures of 90/60 mmHg, and a systolic duration of 400 ms. Average flow rates were measured at the inlet and outlet of the model using ultrasonic flow probes (Transonic Systems, Inc., Millis, MA). All pressures were obtained using Maxxim Medical pressure transducers (Maxxim Medical, Athens, TX). Signals were converted and displayed using a WaveBook acquisition system and WaveView software (IOtech, Inc., Cleveland, OH).

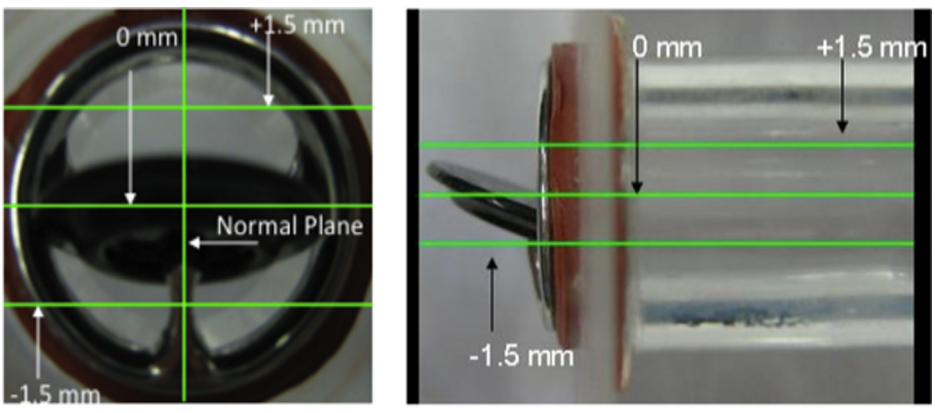


(*a*) (*b*)

**Fig. 3 Bjork-Shiley valve showing four planes of interest (*a*). Side view of valve showing the planes as they are taken in the study (*b*).**

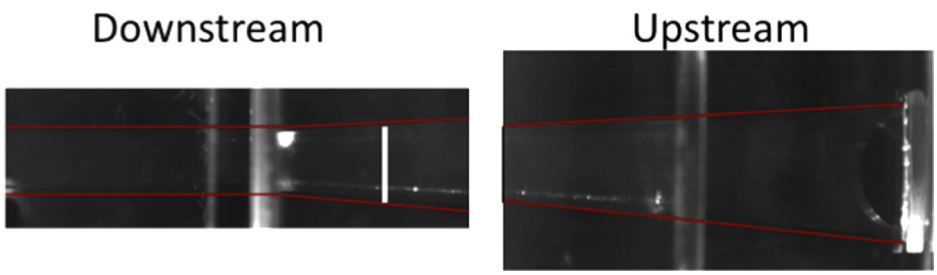


**Fig. 4 Highlighted upstream and downstream raw images showing the portions of the acrylic model that were imaged. The white line in the downstream view represents the overlap between the two field of views and correlates with the left-edge of the upstream image.**

The blood analogs had the properties of pediatric blood with a 40% hematocrit (40 HCT) and goat blood with a 20% hematocrit (Fig. 1). The index of refraction of both fluids matched that of the acrylic model (1.488). The pediatric blood analog was made from xanthan gum (0.03%), glycerin (16%), sodium iodide (50%), and water (33.97%) and is described by Long et al. The goat blood analog made with glycerin (14%), sodium iodide (53.5%), and water (32.5%) and has no elasticity.

Dual Nd:YAG lasers, part of the Gemini PIV 15 system (New Wave Research, Inc., Fremont, CA), were used to produce a 6 mm diameter beam as the light source. The beam was formed into a $\sim$300 $\mu$m thick light sheet by using a $-25$ mm cylindrical lens coupled with a 25 mm diameter high-energy mirror and a 500 mm spherical lens. Two hundred PIV image pairs were acquired using a one megapixel charged-coupled device (CCD) camera (TSI, Inc., Shoreview, MN) with a Micro-Nikkor 60mm f/2.8D lens (Nikon Corporation, Tokyo, Japan). The camera contains a $1000 \times 1016$ pixels CCD chip with a 9 $\mu$m/pixel square spacing. The laser system used was a LaserPulse Synchronizer (TSI, Inc., Shoreview, MN). Both the laser and the camera were controlled using Insight$^{TM}$ 6 software (TSI, Inc., Shoreview, MN). A frame straddling technique was used and the camera was triggered from the beginning of diastole. Two hundred images were taken every 25 ms throughout systole for both 50 and 75 bpm. The fluid was seeded with 10 micron hollow glass spheres (Potters Industries Inc., Valley Forge, PA) to act as tracers for the PIV measurements.

The PIV images were taken at several planes within the model (Fig. 3). First, the model was set so the valve strut was orthogonal to the surface supporting the model. PIV images were taken at the centerline (0 mm), 1.5 mm above the centerline (+1.5 mm), and 1.5 mm below the centerline (−1.5 mm). Then, the model was rotated 90 so the valve strut was now parallel to the surface supporting the model. Three additional planes of data were taken at the same locations at or about the centerline. Data was taken at two fields of view, an upstream field of view ranging from the valve to the 45 mm midline down the decreasing diameter and a downstream field of view ranging from the 45 mm midline down the decreasing diameter into the straight cannula section of the model. These planes were consistent for both models to permit comparison of the different fluid velocity maps at different locations in the model and to examine the effects that changing hematocrit and changing diameter has on fluid flow.

PIV images were masked using a Matlab® 7.1 (The MathWorks, Inc., Natick, MA) program in order to separate the model from the background image. The images were then processed using Insight$^{TM}$ 3G software (TSI, Inc., Shoreview, MN). This program cross-correlates the two images taken at a known time step apart, which is defined as the pulse delay. The pulse delay used varied between 50 $\mu$s and 200 $\mu$s depending on the peak velocity. A deformation grid was used, with a starting interrogation region of $32 \times 32$ pixels and a final region of $16 \times 16$. The Hart Correlation algorithm was used for cross correlation because of its efficient use of extra information garnered from correlation algorithms that overlap interrogation regions [19]. The particle velocities can be calculated by dividing the average particle displacement (pixel resolution 41.6 micons/pixel) by the pulse delay.

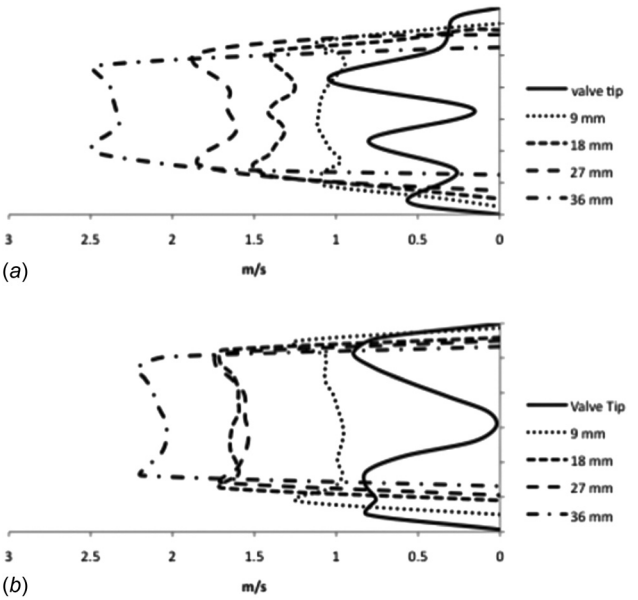


**Fig. 5 Upstream peak velocities during the systolic cycle at the centerline plane of the 40 HCT blood analog (*a*) and the goat blood analog (*b*) at 75 bpm in 6 mm model**

## 3 Results and Discussion

The upstream and downstream field of views, with a slight overlap at the white line, are shown in Fig. 4. Velocity profiles shown are representative of the flow through the aortic cannula. The fluid is flowing from right to left in the figures as it leaves the PVAD and moves through the cannula.

Figure 5, taken at the centerline at peak velocity (2.5 m/s), shows differences between the 40 HCT blood analog and the goat blood analog in the 6 mm model. Immediately after the valve in the 40 HCT blood analog, the wakes are quite different between the fluids where 40 HCT shows a more complex flow. The MHV strut wake is more pronounced and decays more slowly for the 40 HCT fluid.

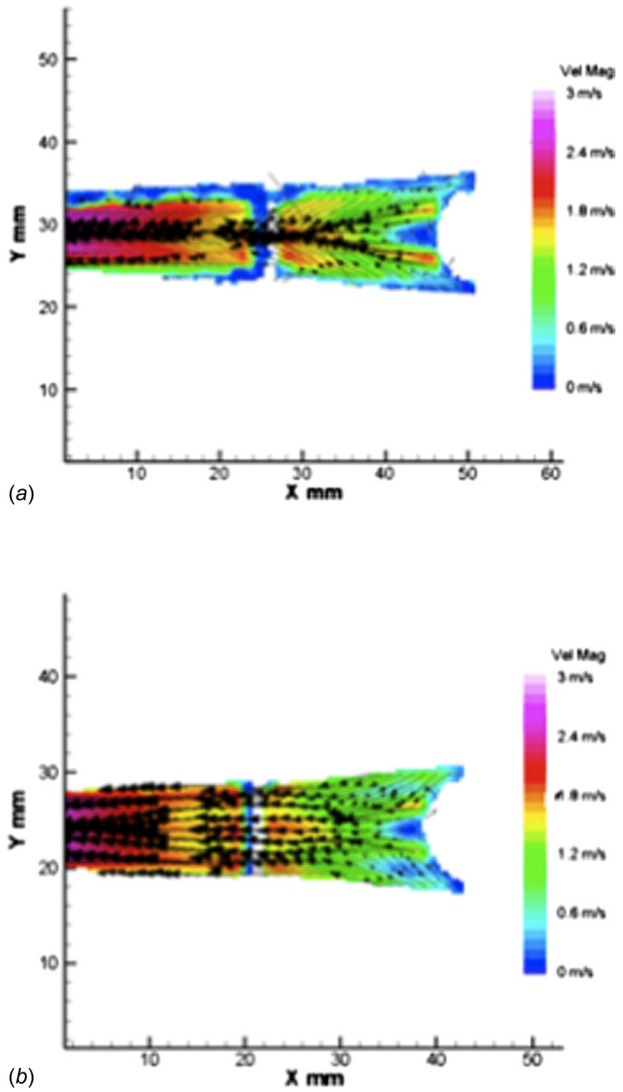


**Fig. 6 Upstream peak velocities during the systolic cycle at the −1.5 mm plane of the 40 HCT blood analog (*a*) and the goat blood analog (*b*).**

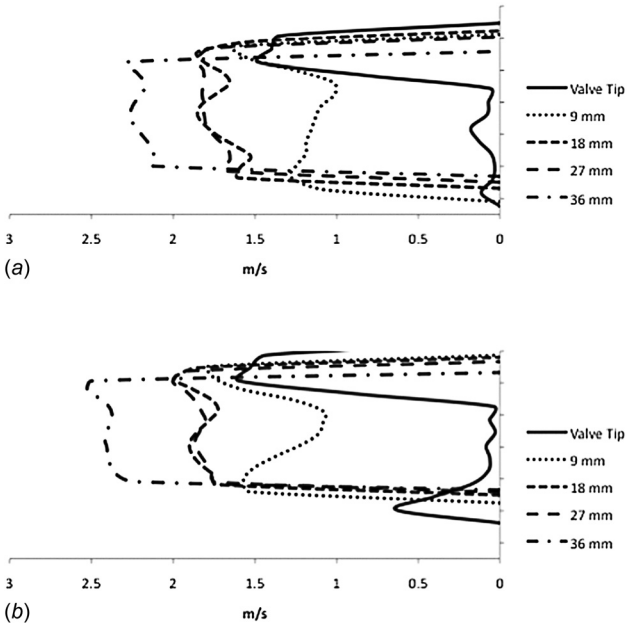


**Fig. 7 Side view peak velocities during the systolic cycle at the centerline plane of the 40 HCT blood analog (*a*) and the goat blood analog (*b*) at 75 bpm in the 6 mm model**

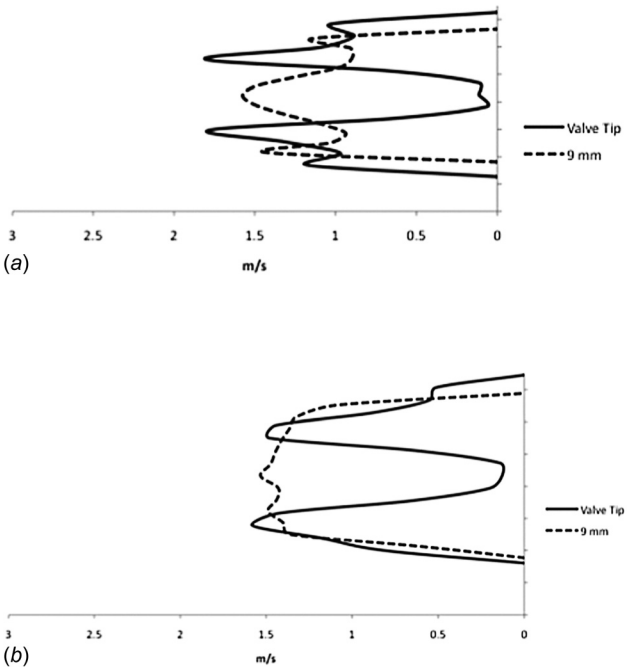


**Fig. 8 Upstream peak velocities during the systolic cycle at the −1.5 mm plane of the 40 HCT blood analog (*a*) and the goat blood analog (*b*) in the 8 mm model**

It is constructive to examine the entire PIV flow field planes as (Fig. 6) they show the fundamental differences between the fluids. There is a strong jet flow in the 40 HCT analog downstream of the valve, which the goat analog does not show. Recall this plane is immediately downstream of the valve strut. Further downstream of the valve, the goat analog shows a more uniform flow than does the 40 HCT analog, which is characterized by a strong central jet. The wall shear stress pattern will be different for the fluids. To support the jet, the flow for the 40 HCT fluid must have significant three dimensionality.

We observe that there are areas of separation near the valve with the 40 HCT analog, which is not occurring with the goat blood analog. These separations occur throughout the entire cycle (not shown) and are areas of concern. In the outlet port (Fig. 2, Sec. 1) near the MHV, a lip is formed that might increase the potential for separation leading to thrombosis. There are large differences in the fluid dynamics between the analogs, as shown in Fig. 7, and these make the interpretation and application of animal implant data challenging.

The downstream field of view (Fig. 2, Sec. 3) again shows differences, albeit minor, between both blood analogs in all three planes (data not shown). The centerline plane taken at peak velocity with the 40 HCT analog has a less uniform profile with a central jet that does not develop with the goat analog.

At 50 bpm, there were only minor differences between the two blood analogs. With a lower flow rate (peak velocity of 1.8 m/s), the overall flow is much slower throughout the entire cycle. The areas of separation that formed at 75 bpm are not seen at 50 bpm.

The differences between the two analogs in the side view images were consistent with the previous data. Figure 7 shows centerline peak velocity (2.6 m/s) of the two blood analogs at 75 bpm. As is clearly shown at the valve tip, the wake flow for both fluids is strongly asymmetric. The goat blood analog shows more rapid recovery from the influence of the valve strut which is

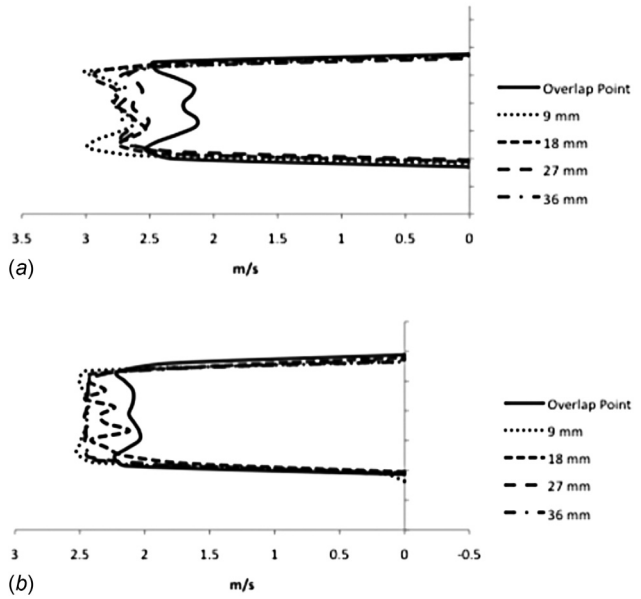


**Fig. 9 Downstream peak velocities during the systolic cycle at the center plane of the 40 HCT blood analog (*a*) and the goat blood analog (*b*) in the 8 mm model at 75 bpm. The overlap point is consistent with Fig. 4.**

correlated to the less viscous behavior and negligible elasticity of the goat blood analog.

Similar trends were seen in the 8 mm model. At peak velocity in the −1.5 mm plane (Fig. 8), there are large differences in the flow profile between the 40 HCT fluid and the goat analog secondary to the minor valve orifice influencing the structure of the wake. The 40 HCT fluid shows a flow convergence immediately downstream of the valve similar to that in the 6 mm model. While the peak velocity are similar between the two fluids, the flow profile of the goat analog is more uniform. Such discrepancies between the blood analogs were observed throughout the entire cycle.

While the 6 mm model shows similar flow patterns between the two fluids in the downstream field of view, the 8 mm model (Fig. 9) shows different flow patterns between the analogs. At the centerline plane, the 40 HCT fluid analog shows flow moving towards the side of the model during peak flow. The flow in the goat analog continues to be uniform.

Similar to the 6 mm model at 50 bpm, the 8 mm model shows little difference at peak velocity between the two fluids. Both fluids have a peak velocity of 1.6 m/s towards the end of the upstream field of view and show a relatively uniform flow pattern with no convergence.

## 4 Conclusions

Differences in hematocrit have a significant effect on the fluid dynamics of blood flow for both the 6 and 8 mm cannulae. When comparing the two models, the 8 mm model showed a more gradual increase in velocities during systole as well as lower peak velocities downstream suggesting, as anticipated, a lower shear. The fluid also developed into a more laminar flow pattern closer to the valve orifice in the 8 mm cannula. The goat blood analog (essentially a Newtonian fluid) has a much more uniform flow; which may decrease the extent of blood damage as it passes through the cannula, by reducing the wall shear and the corresponding pressure drop. The areas of separation for the pediatric blood analog are of concern because they will lead to thrombosis. The flow into the aorta is likely to be quite different for the two analogs. The rheology of goat and human blood are quite different. Human blood at 40% hematocrit; for example, has significant shear thinning and a measurable elasticity. Goat blood is significantly less viscous, even at high strain rates, and has no measurable elastic component. The differences are principally a reflection of the lack of rouleaux formation for goat blood at its lower hematocrit. As we have previously observed in blood pumps, the higher viscosity and elasticity of human blood produce more persistent coherent fluid structures—jets and wakes, here. These persistent fluid motions alter the overall flow patterns between goat and human blood in the cannula, particularly at the higher flow rates. Three dimensionality, strong coherent jets and separated regions, which appear in the 40% hematocrit flow field, are not mimicked by the goat analog, independent on the cannula sizes we have studied.

Thrombosis in artificial devices is characterized by a complex interaction between the biochemical state of the blood, the nature of the artificial material and the local fluid mechanics. The use of animal models will always represent a compromise on the state of the blood, but here, the use of a goat as the animal model also compromises on the state of the local fluid mechanics. This study points out that animal studies are probably not sufficient on their own in identifying the thrombogenicity of cannulae, and that such animal data would more be readily interpreted in concert with bench and computational studies in which the viscoelastic nature of the blood is suitably modeled.

## Acknowledgment

This study was supported by NIH – NHLBI Contract No. HV 48191 and the ARL Exploratory and Foundational Graduate Student Research Program.

## References

[1] Baldwin, J. T., Borovetz, H. S., Duncan, B. W., Gartner, M. J., Jarvik, R. K., Weiss, W. J., and Hoke, T. R., 2006, "The National Heart, Lung, and Blood Institute Pediatric Circulatory Support Program," Circulation, **113**, pp. 147–155.

[2] Frazier, O. H., and Myers, T. J., 1999, "Left Ventricular Assist System as a Bridge to Myocardial Recovery," Ann. Thorac. Surg., **68**, pp. 734–741.

[3] Mancini, D. M., Beniaminovitz, A., Levin, H., Catanese, K., Flannery, M., DiTullio, M., Savin, S., Cordisco, M. E., Rose, E., and Oz, M., 1998, "Low Incidence of Myocardial Recovery After Left Ventricular Assist Device Implantation in Patients With Chronic Heart Failure," Circulation, **98**, pp. 2383–2389.

[4] Frazier, O. H., Benedict, C. R., Radovancevic, B., Bick, R. J., Capek, P., Springer, W. E., Macris, M. P., Delgado, R., and Buja, L. M., 1996, "Improved Left Ventricular Function After Chronic Left Ventricular Unloading," Ann. Thorac. Surg., **62**, pp. 675–682.

[5] Zimmerman, H., Covington, D., Smith, R., Inaht, C., Barber, B., and Copeland, J., 2010, "Recovery of Dilated Cardiomyopathies in Infants and Children Using Left Ventricular Assist Devices," ASAIO J., **56**, pp. 364–368.

[6] Cassidy, J., Haynes, S., Kirk, R., Crossland, D., Smith, J. H., Hamilton, L., Griselli, M., and Hasan, A., 2009, "Changing Patterns of Bridging to Heart Transplantation in Children," J. Heart Lung Transplant, **28**, pp. 249–54.

[7] Arabia, F. A., Tsau, P. H., Smith, R. G., Nolan, P. E., Paramesh, V., Bose, R. K., Woolley, D. S., Sethi, G. K., Rhenman, B. E., and Copeland, J. G., 2006, "Pediatric Bridge to Heart Transplantation: Application of the Berlin Heart, Medos and Thoratec Ventricular Assist Devices," J. Heart Lung Transplant, **25**, pp. 16–21.

[8] Ando, Y., Kitao, T., Nagaoka, E., Kimura, T., Yokoyama, Y., Yoshikawa, M., Tominaga, R., and Takatani, S., 2011, "One-Month Biocompatibility Evaluation of the Pediatric TinyPump in Goats," Artif. Organs, **35**(8), pp. 813–818.

[9] Yang, N., Deutsch, S., Paterson, E. G., and Manning, K. B., 2010, "Hemodynamics of an End-to-Side Anastomotic Graft for a Pulsatile Pediatric Ventricular Assist Device," J. Biomech. Eng., **132**, pp. 031009-1–031009-13.

[10] Long, J. A., Undar, A., Manning, K. B., and Deutsch, S., 2005, "Viscoelasticity of Pediatric Blood and its Implications for the Testing of a Pulsatile Pediatric Blood Pump," ASAIO J., **51**, pp. 563–566.

[11] Undar, A., Ji, B., Rider, A., Lukic, B., Kunselman, A. R., Weiss, W. J., and Myers, J. L., 2007, "Comparison of Four Different Pediatric 10F Aortic Cannulae During Pulsatile Versus Nonpulsatile Perfusion in a Simulated Neonatal Model of Cardiopulmonary Bypass," ASAIO J., **53**, pp. 778–784.

[12] Mareels, G., Kaminsky, R., Eloot, S., and Verdonck, P. R., 2007, "Particle Image Velocimetry Validated, Computational Fluid Dynamics Based Design to Reduce Shear Stress and Residence Time in Central Venous Hemodialysis Catheters," ASAIO J., **53**, pp. 438–446.

[13] Muehrcke, D. D., Cornhill, J. F., Thomas, J. D., and Cosgrove, D. M., 1995, "Flow Characteristics of Aortic Cannulae," J. Card. Surg., **10**(4), pp. 514–519.

[14] De Paulis, R., Engelhardt, H., Chiariello, L., Reul, H., and Morea, M., 1990, "*In Vitro* Evaluation of Left Ventricular Assistance by Cannulation of Both Femoral Arteries," Int. J. Art. Org., **13**(4), pp. 237–246.

[15] De Wachter, D., De Somer, F., and Verdonck, P., 2002, "Hemodynamic Comparison of Two Different Pediatric Aortic Cannulas," Int. J. Art. Org., **25**(9), pp. 867–874.
[16] Hetzer, R., Potapov, E. V., Stiller, B., Weng, Y., Hubler, M., Lemmer, J., Alexi-Meskishvili, V., Redlin, M., Merkle, F., Kaufmann, F., and Hennig, E., 2006, "Improvement in Survival After Mechanical Circulatory Support With Pneumatic Pulsatile Ventricular Assist Devices in Pediatric Patients," Ann. Thorac. Surg., **82**, pp. 917–925.
[17] Yang, N., Deutsch, S., Paterson, E. G., and Manning, K. B., 2009, "Numerical Study of Blood Flow at the End-to-side Anastomosis of a Left Ventricular Assist Device for Adult Patients," J. Biomech. Eng., **131**(11), pp. 111005-1–111005-9
[18] Rosenberg, G., Phillips, W. M., and Landis, D. L., 1981, "Design and Evaluation of the Pennsylvania State University Mock Circulatory System," ASAIO J., **4**, pp. 41–49.
[19] Hart, D. P., 1998, "High-Speed PIV Analysis Using Compressed Image Correlation," J. Fluids Eng., **120**, pp. 463–470.